


UGPS J194310+183851: an unusual optical and X-ray faint cataclysmic variable?

C. Morris ^{1,★}, T. J. Maccarone,² P. W. Lucas ¹, J. Strader,³ C. T. Britt,⁴ N. Miller,¹ S. J. Swihart,^{5,6} W. J. Cooper ^{1,7}, J. E. Drew ^{1,8} and Z. Guo ^{1,9,10}

¹Centre for Astrophysics Research, University of Hertfordshire, College Lane, Hatfield, Hertfordshire AL10 9AB, UK

²Department of Physics and Astronomy, Texas Tech University, Box 41051, Lubbock, TX 79409-1051, USA

³Center for Data Intensive and Time Domain Astronomy, Department of Physics and Astronomy, Michigan State University, East Lansing, MI 48824, USA

⁴Space Telescope Science Institute, 3700 San Martin Dr, Baltimore, MD 21218, USA

⁵National Research Council Research Associate, National Academy of Sciences, Washington, DC 20001, USA

⁶Resident at Naval Research Laboratory, Washington, DC 20375, USA

⁷Istituto Nazionale di Astrofisica, Osservatorio Astrofisico di Torino, Strada Osservatorio 20, I-10025 Pino Torinese, Italy

⁸Department of Physics and Astronomy, University College London, Gower Street, London WC1E 6BT, UK

⁹Instituto de Física y Astronomía, Universidad de Valparaíso, Avenida Gran Bretaña 1111, Casilla 5030, Valparaíso, Chile

¹⁰Núcleo Milenio de Formación Planetaria (NPF), Casilla 5030, Chile

Accepted 2022 June 13. Received 2022 May 30; in original form 2022 February 28

ABSTRACT

The growing number of multi-epoch optical and infrared sky surveys are uncovering unprecedented numbers of new variable stars, of an increasing number of types. The short interval between observations in adjacent near-infrared filters in the UKIDSS Galactic Plane Survey (UGPS) allows for the discovery of variability on the time-scale of minutes. We report on the nature of one such object, through the use of optical spectroscopy, time series photometry, and targeted X-ray observations. We propose that UGPS J194310.32+183851.8 is a magnetic cataclysmic variable star of novel character, probably featuring a longer than average spin period and an orbital period likely to be shorter than the period gap (i.e. $P_{\text{orb}} < 2$ h). We reason that the star is likely a member of the short-period intermediate-polar subclass that exists below this period boundary, but with the additional feature that system’s spectral energy distribution is fainter and redder than other members of the group.

Key words: stars: individual: UGPS J194310.32+183851.8 – novae, cataclysmic variables – stars: peculiar – stars: variables: general.

1 INTRODUCTION

The object UGPS J194310.32+183851.8 (hereafter referred to as Source 363; Lucas et al. 2017) was imaged twice as part of the UKIDSS Galactic Plane Survey (UGPS), displaying 1.97 mag infrared (IR) variability in K over the 4 yr interval and $H\alpha$ emission in the INT Photometric H-Alpha Survey (IPHAS) photometry (Drew et al. 2005). One of the IR colours was exceptionally blue: $J - H = -0.6$, but $H - K = +0.7$. Lucas et al. (2017) suggested that this might be due to variability on the 7 min time-scale of the UKIRT Infrared Deep Sky Survey (UKIDSS) filter changes, supported by marginal detections in the Two Micron All-Sky Survey (2MASS) images that suggested unremarkable colours. Additionally, the *Gaia* satellite has determined a fairly nearby location (see Section 2.1). Consequently, from the lack of any previous detection of hard X-rays, gamma-rays, or radio waves by facilities such as the *Fermi*-Large Area Telescope (LAT), the *ROentgen SATellite* (ROSAT), and the Very Large Array Sky Survey (VLASS; Voges et al. 1999; Atwood et al. 2009; Lacy et al. 2020), we infer that the system does not contain a

neutron star or black hole. Thus we must be looking at a white dwarf (WD) binary system most likely of the cataclysmic variable (CV) type.

CVs are binary systems containing a WD and a close companion (of comparatively low mass), wherein the WD primary accretes mass via Roche lobe overflow from the secondary star (see Knigge, Baraffe & Patterson 2011; Schreiber et al. 2021, for comprehensive reviews). These systems are subdivided into magnetized and unmagnetized systems (based largely on the presence or absence of pulsations caused by the accretion flow proceeding along the magnetic field lines), and further subdivided based upon the method of WD accretion. The magnetic CVs consist of polars and intermediate polars (IPs). Polars accrete matter following the magnetic field lines directly to the surface of the primary due to their high magnetic field strengths of 7–230 MG (Oliveira et al. 2017). This high field strength also causes the orbit and the spin of the WD’s magnetosphere to become synchronous. In contrast, in IPs the Alfvén radius is smaller than the circularization radius of the accretion disc, but larger than the WD’s radius, allowing an outer disc to exist. This disc is truncated, and then leads to the flow following magnetic field lines at free-fall velocity in the inner region. These systems are also notable for the spin and orbital periods (P_{spin} and P_{orb}) being different from one

* E-mail: c.morris6@herts.ac.uk

another. It should be noted that a small subgroup of IPs can transfer mass via both disc-fed and stream-fed methods; for example FO Aqr, TX Col (Littlefield et al. 2020, 2021), and others still are known to be solely stream-fed and are referred to as discless IPs, such as EX Hya and DW Cnc (Rodríguez-Gil et al. 2004; Andronov & Breus 2013).

Their hard spectrum arises because the gas is in free-fall on to a WD, so if the accretion column is optically thin, the emission will come out as bremsstrahlung radiation with energies $E \approx kT \sim 10\text{--}30$ keV. The innermost region will usually be optically thick, and then can give emission in soft X-rays or extreme ultraviolet (EUV), depending on the luminosity and the size scale of the polar region spot at the base of the accretion column. It is reasonable that some of these are missed because of absorption effects, but that is still unsettled. X-ray spectra frequently show ionized iron in emission, caused by shock excitation from the free-falling disc material.

In the optical regime, the systems are highly variable and multiperiodic, with periodicities associated with the WD spin, the binary orbit, and beat interactions between these two periods. Spectrally, IPs are characterized by broad emission of hydrogen recombination lines, as well as emission of helium (both neutral and ionized), carbon, and nitrogen. Absorption features can be used to understand the composition of the companion [providing they are of high signal-to-noise ratios (S/Ns)], as well as the disc inclination. By comparison, polars have stronger but narrower emission features (often having Zeeman splitting due to the high magnetic field strength), including a prominent doubly ionized nitrogen line at 4650 Å produced in the accretion column.

In this paper, we present the discovery of Source 363's nature as a new magnetic CV. We report on optical spectroscopic observations showing unusually broad emission lines (Section 3.1). We then detail numerous photometric monitoring observations that illustrate the system's behaviour on short time-scales (Section 3.2), revealing periodicity at ≈ 2760 s. Finally, we report on new X-ray observations by the *Neil Gehrels Swift Observatory* (hereafter *Swift*) that have provided the first detections of X-ray emission from the source, consistent with our classification of the source as an accreting WD system (Section 3.3). We then conclude with a discussion on the nature and novel properties of the source, given the various dichotomies our combined approach has uncovered (Section 4).

2 SOURCE INFORMATION AND OBSERVATIONS

2.1 Source characteristics

Previous optical and IR observations of the source have been carried out as part of UGPS, 2MASS, UVEX, IPHAS, *Gaia*, and Panoramic Survey Telescope and Rapid Response System (Pan-STARRS; Drew et al. 2005; Skrutskie et al. 2006; Lucas et al. 2008; Groot et al. 2009; Flewelling 2017; *Gaia* Collaboration et al. 2018, 2021). They reveal the source to be an optically faint but comparatively IR-bright variable star (see Table 1), with a prominent H α excess. Rapid variability is clearly seen in the sparsely sampled Pan-STARRS 1 optical light curve: it varies by a factor of 4 in 15 min or less in r , confirming the fast nature of the source's variability. This indicates that the system includes a compact object of some type. The latest distance from Bailer-Jones et al. (2021) using *Gaia* Early Data Release 3 (EDR3) put the star at $900.7^{+288.3}_{-245.6}$ pc, which leads to an absolute magnitude in G of 10.61, although some care should be taken with this due to the variability of the source, as the prior used by Bailer-Jones et al. (2021) is more suited to non-variable stars. All these features together were indicative of Source 363 possibly being

a compact object, although there was no associated X-ray emission recorded in previous all-sky surveys, so the flux must be less than 5×10^{-13} erg cm $^{-2}$ s $^{-1}$, the limit for *ROSAT* (Voges et al. 1999). The absence of X-rays of the required intensity can safely rule out a neutron star system, but a CV system would still be plausible for a faint X-ray source. The combination of the strong, rapid variability (seen in Fig. 1) and the lack of X-ray emission in all-sky surveys led to the acquisition of targeted X-ray observations, several high-cadence light curves, and an optical spectrum.

2.2 SOAR observations

2.2.1 Spectroscopy

We obtained a single low-resolution spectrum of the source on 2021 May 12 with the Red Camera of the Goodman Spectrograph (Clemens, Crain & Anderson 2004) on the SOUTHERN Astrophysical Research (SOAR) telescope. The exposure time was 1800 s, and the observation used a 400 lines mm $^{-1}$ grating and a 0.95 arcsec slit together with a GG395 longpass filter, yielding a full width at half-maximum resolution of 5.4 Å (about 250 km s $^{-1}$) over a usable wavelength range $\sim 4000\text{--}7820$ Å.

The spectrum was reduced and optimally extracted in the usual manner using IRAF (Tody 1986). The resulting spectrum has an average S/N of ~ 14 per resolution element (~ 8 pixel $^{-1}$) in the continuum. The spectrum and selected line profiles can be seen in Figures 2 & 3 respectively.

2.2.2 Imaging

Follow-up imaging was obtained on 2021 June 9, using the Red Camera of SOAR/Goodman in imaging mode. We obtained 29 exposures, each of 180 s duration, using the Sloan Digital Sky Survey (SDSS) i' filter. These totalled 87 min on source over a time span of 98 min. The average airmass was 1.62 and typical seeing was 1.5 arcsec.

The raw images were corrected for bias and then flat-fielded with sky flats using standard routines in IRAF (Tody 1986). We performed differential photometry of Source 363 with respect to 17 nearby, non-variable stars and calibrated these magnitudes using their Pan-STARRS Data Release 2 (DR2; Chambers et al. 2016) i' mag, the final results can be seen in Fig. 4.

2.3 WHT observations

We made use of recently offered service time on the William Herschel Telescope (WHT) for testing the new PF-QHY camera¹ to obtain two high-cadence light curves. These were using Sloan u' and r' filters, with 62 and 61 epochs of data covering 90 and 89 min, respectively, and individual exposures of 80 s in each band. PF-QHY is a wide-field camera with a complementary metal oxide semiconductor (CMOS) detector, its field of view being 10.7×7.1 arcmin 2 and a pixel scale of 0.267 arcsec using 4×4 binning. Data reduction and calibration were carried out using the PHOTUTILS (Bradley et al. 2021) and ASTROPY (Astropy Collaboration et al. 2013, 2018) libraries for PYTHON, with profile-fitting photometry being used in the crowded r' images. Aperture photometry was used in the u' images as the field is comparatively less populated with sources. Calibration was done via

¹See the instrument page for details: '<http://www.ing.iac.es/astronomy/instruments/pf-qhy/>'

Table 1. Selected archival measurements for Source 363.

Survey	Filter	Mean magnitude and error	No. of epochs	Maximum variation (mag)
UKIDSS [1]	K_s	16.70 ± 0.08	2	1.97
UKIDSS [1]	H	18.36 ± 0.11	1	N/A
UKIDSS [1]	J	17.76 ± 0.03	1	N/A
IGAPS [2]	r	20.54 ± 0.06	4	1.94
IGAPS [2]	$H\alpha$	19.42 ± 0.06	2	N/A
IGAPS [2]	i	19.27 ± 0.07	2	N/A
IGAPS [2]	RGO U	19.68 ± 0.03	2	0.37
<i>Gaia</i> [3]	G	20.02 ± 0.10	3	0.72
Pan-STARRS [4]	g	20.35 ± 0.04	8 ^a	1.46
Pan-STARRS [4]	r	20.83 ± 0.07	8	1.82
Pan-STARRS [4]	z	19.64 ± 0.07	4 ^a	0.55

Note. References: [1]: Lucas et al. (2008) and Contreras Peña et al. (2014); [2]: Monguió et al. (2020); [3]: Gaia Collaboration et al. (2016, 2018, 2021); and [4]: Flewelling (2017). ^aMore epochs were available but they are not included because of poor data quality.

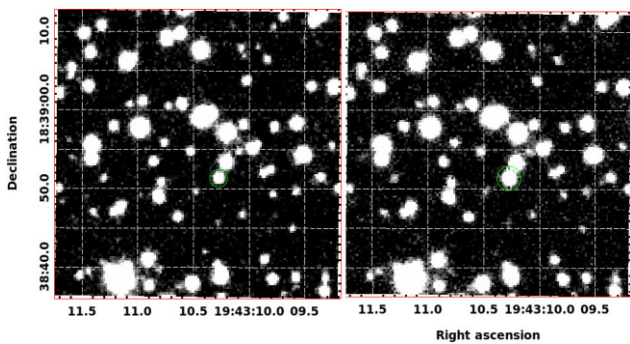


Figure 1. William Herschel Telescope (WHT) PF-QHY r' -band images of Source 363 (within the green annulus), showing the short time-scale variation, with the 1.1 mag change across 16 min. The left-hand panel has an MJD of 59386.153 and the right-hand panel of 59386.164.

a standard star SP 1942+261, with corrections to individual epochs being averaged across non-variable stars in each frame.

2.4 *Swift* XRT/UVOT observations

We obtained X-ray and ultraviolet (UV) data from *Swift* via a successful target of opportunity (ToO) program on the 2021 July 2, using both the X-Ray Telescope (XRT) and UltraViolet and Optical Telescope (UVOT) instruments in parallel, with 4 ks of observation in the photon-counting mode. These data produced the standard X-ray images, light curve, and spectrum, as well as additional images and a light curve in the UVOT U filter. The data were provided pre-reduced via the *Swift* ToO server (Evans et al. 2009, 2020) with the spectrum being fitted with a power law, and adjusted for galactic absorption along the line of sight. Calibration for the UVOT data was done in PYTHON using the same packages described previously. All other XRT reduction was carried out using XSPEC, using the specific set-up for *Swift*-XRT.

3 RESULTS AND ANALYSIS

3.1 Optical spectrum

The SOAR spectrum (Fig. 2) displays a number of features consistent with CVs in general, most notably $H\alpha$ and $H\beta$ in emission, with additional emission features from both neutral and singly ionized helium (see Table 2 for details of individual lines). All emission

lines are broad and single peaked, with a wavelength resolution of 100.5 km s^{-1} at 5910 \AA (the mid-point of the spectrum). The wide range of velocities suggests the presence of a disc, or possibly a symmetric wind, although this cannot be further identified due to the blending of any C III/N III lines into the wings of the He II line at 4686 \AA . Fitting of line profiles (using a Voigt profile to account for both Doppler and Stark broadening) provides an average radial velocity (RV) of $-280.2 \pm 12.9 \text{ km s}^{-1}$ (see Fig. 3). This value, while high, is not unexpected when only one spectrum is available, and the system's mean RV is likely less than this. Some absorption features could be present in the spectrum, however the modest S/N (≈ 14 per resolution element) precludes any reliable identification of these, and thus we have to determine the characteristics of the companion star through another method.

From the equivalent width (EW) ratio of $\text{He II}/H\beta = 0.18 \pm 0.10$ we cannot be certain whether the system's accretion is primarily magnetic (see Silber 1992), due to the noise in the detection of the He II line: a ratio above 0.4 is indicative of magnetically controlled accretion. It should be noted that those authors also suggest that the EW of $H\beta$ should be $\geq 20 \text{ \AA}$ in magnetic systems: here we have $\text{EW} = 49.3 \text{ \AA}$. We reason that the observed hydrogen line ratios may be as a result of a more complete than usual disc (for an IP), bearing resemblance to those observed around dwarf novae. In those cases the slower rotating outer disc regions limit the excitation of the more energetic recombination lines, leading to lower fluxes from $H\beta$ and $H\gamma$ than normal IPs.

We cannot be sure if Source 363 was in a brighter than average state at the time of observation; pre-spectroscopic imaging places the star at an intermediate-brightness level (compared to its maxima and minima). However we cannot interpret whether the star was pre- or post-outburst, which given the length of the subsequent observation could place the star at either state. This is especially true given the low S/N of the He II line, meaning that the true ratio might be higher than the 0.4 value that is assumed to indicate magnetized accretion.

In comparison to objects from the literature, we note the absence of emission from N III and C III, which is commonly seen in fully magnetic polars (Warner 1995). In addition the fringes of the $H\beta$ line do not contain the characteristic absorption features that are associated with a high disc inclination angle. Given that a broad range of velocities is observed the disc inclination angle cannot be very low so we can reason that the inclination angle is intermediate. The same line can also show the hallmarks of cyclotron radiation, as an overall increase in the localized continuum, which we note that Source 363 does not display, so cyclotron

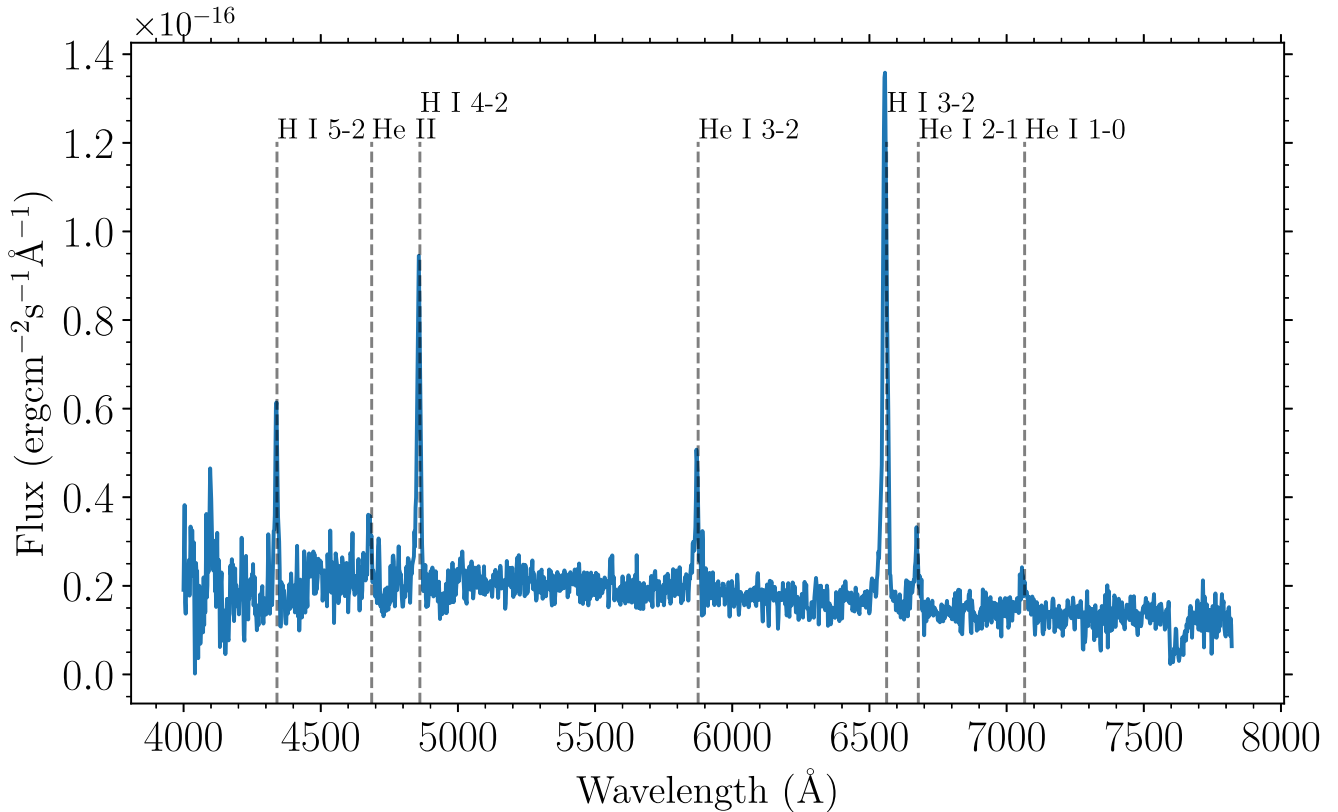


Figure 2. Optical spectrum of Source 363, using the Goodman Spectrograph at SOAR. Hydrogen recombination lines are prominent, and broader than those seen in more typical CVs. Other common CV lines such as He I and He II are also present, although the 4606 Å Na III line often associated with IPs is not seen above the noise.

Table 2. Equivalent line widths for notable features in the I -band spectrum. While faint absorption features from a companion star can possibly be seen, they are not prominent enough for us to provide analysis. It is worth noting the approximate 9/3/1 ratio between the Balmer lines, while the helium ground-state transitions indicate a higher population at higher energy levels, with the 3–2 line being most prominent. The helium lines were affected by noise and some blending, and thus have not been fitted for radial velocities (RVs) and widths.

Emission line	Equivalent width and error (Å)	Width (km s ⁻¹)
H I 4340 Å (5–2)	-21.7 ± 5.7	1746.6
H I 4861 Å (4–2)	-49.3 ± 2.6	2302.9
H I 6562 Å (3–2)	-161.6 ± 2.2	2747.5
He I 5875 Å (3–2)	-31.3 ± 4.2	N/A
He I 6678 Å (2–1)	-19.4 ± 5.2	N/A
He I 7065 Å (1–0)	-16.2 ± 4.9	N/A
He II 4685.7 Å	-9.0 ± 5.1	N/A

radiation is unlikely to be the cause of the observed near-IR excess.

3.2 Light curves

The three light curves (Figs 4, 5, and 6 for u' , r' , and i' , respectively) each display amplitudes between 0.9 and 1.2 mag, but each wavelength shows differing behaviour: the u' curve shows symmetric

behaviour with minimal time spent at either bright or faint states, whereas the r' curve is at a faint level for approximately two-thirds of the observation, with the rise taking ≈ 7 min, followed by a 20 min decline to a state of quiescence, resembling behaviour reminiscent of stream-fed accretion on to the WD. This is similar to that seen in polar-type magnetic CVs (mCVs). The longer duration observations in i' show two peaks, with a separation and shape consistent with the u' data, including the scatter about the curves' minima. The peaks are separated by 51 ± 2.2 min and 65 ± 2.1 min for i' and u' , respectively, with the r' curve having a less clear cycle, although the curves' minima are separated by $\approx 64 \pm 2.1$ min. These estimates provide a rough baseline for the most visible time-scales of variability.

The u' and i' light curves show small amplitude variation at low-brightness states not seen at the maxima, although at this time it cannot be wholly rejected that these are indicators of short period variability (not unlikely given the magnetohydrodynamic processes present in the disc). We investigated this by fitting a third-order spline to the phase-folded light curve (using SCIPY; Virtanen et al. 2020) and checking the residuals to this fit. This revealed no obvious periodicity. It would seem therefore that the variations during the system's minima are more likely the result of increased sensitivity to the atmospheric conditions during the observations. In addition a 19 h light curve (with approximately 1 h on-source) in UVOT U band was produced, consisting of six epochs of varying exposure time. Whilst not much can be gleaned from the shape (given the known rate of variability), the maximum amplitude was ≈ 0.8 mag, in keeping with data from other bands.

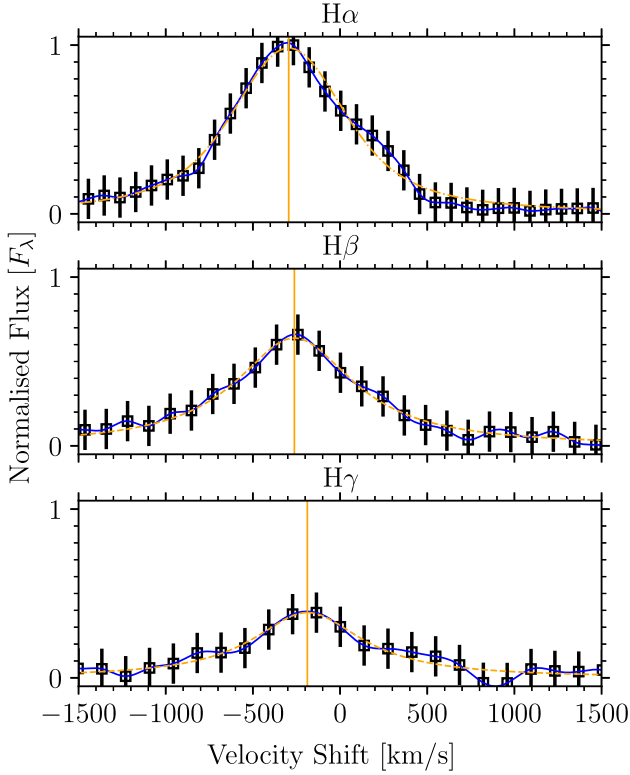


Figure 3. Fitted line profiles and radial velocities for the hydrogen recombination lines. Points and blue lines are the data, yellow dashed lines are the fits, using a Voigt profile, and converted into velocity space. The median radial velocity (RV) of the star was $-283.9 \pm 9.3 \text{ km s}^{-1}$, relative to the local standard of rest. The individual radial velocities fitted to each line are marked with solid yellow lines. Fluxes are normalized with respect to the H13 \rightarrow 2 line.

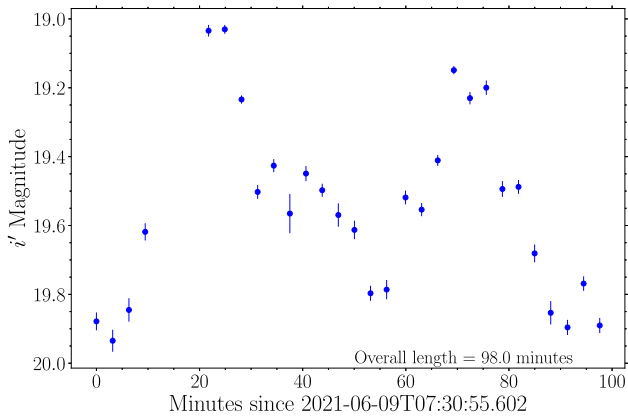


Figure 4. i' -band light curve for Source 363, using SOAR's Goodman Spectrograph in imaging mode. Fainter exposures were averaged with sequential epochs to recover signal. The peaks are separated by $\approx 51 \pm 2.2$ min and the amplitudes are ≈ 0.9 mag.

Interpreting the nature of the observed variability is a challenge due to the limited time span of the observations, although a few causes can be inferred. A common cause of variability in CVs is flickering, a phenomenon that is thought to relate to modulation of the accretion rate and flares associated therein (see Bruch 2021 for a comprehensive review). A second driver of variability could be the spin of the WD primary star, seen via the accretion columns or

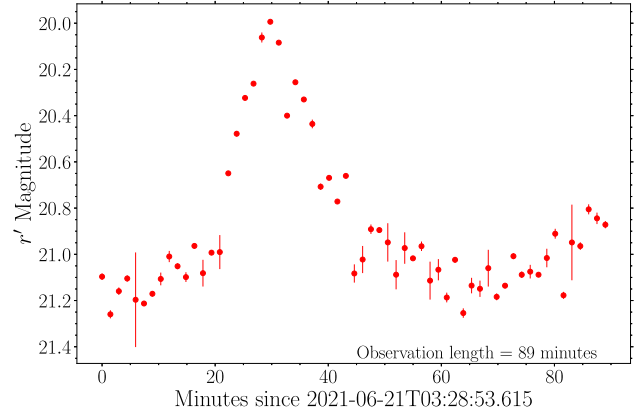


Figure 5. r' -band light curve, obtained with the PF-QHY instrument on the WHT. The peak shows an amplitude of ≈ 1.2 mag and resembles flare-like behaviour, with a comparatively fast rise followed by extended cooling time. If we assume this behaviour repeats based upon data from other filters, the time-scale is of the order of approximately 66 min, from the start of the event to the next rise.

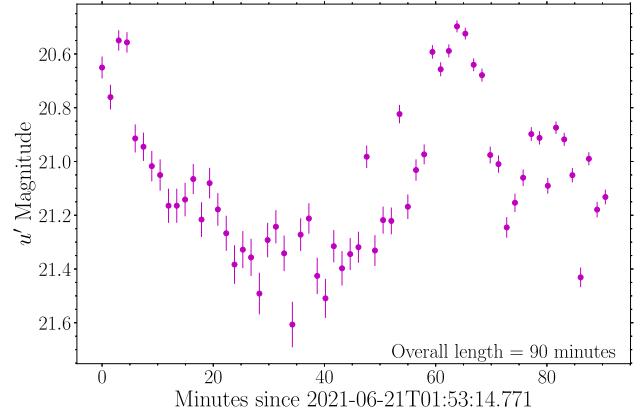


Figure 6. u' -band light curve, obtained with the PF-QHY instrument on the WHT. There is significant scatter in this curve, likely because of the u' bands increased sensitivity to changes in seeing. However, the same high amplitude, short time-scale behaviour can be seen as in other filters. The two apparent peaks are separated by between 64 and 67 min, which is analogous to the time-scales seen in the r' curve.

polar hotspots (depending on observed wavelength). A complication can arise from the orbital sideband: a sideband represents the reprocessing of the WD primary's emission by its disc, which causes an interaction between the spin period and the orbital period of the secondary, observed as a distinct frequency, $\omega_{\text{spin}} \pm \omega_{\text{orb}}$, with a positive sign in most in cases, e.g. AO Psc (Bonnardeau 2015), and a negative sign if the orbit is retrograde. While there are currently not enough individual cycles to confirm any periods, we note that the lack of observed periodicities at short time-scales (≈ 20 min) in any of the curves is interesting. This could imply that the WD does not spin at the common period of approximately 10–15 min.

3.3 X-ray photometry

The *Swift*-XRT observations detect a single source at RA = 295^o.7935 and Dec. = 18^o.6475 with an astrometric uncertainty of 3.0 arcsec (see Fig. 7) given by the *Swift*-XRT data products generator' software (Evans et al. 2014). These coordinates are offset from the optical/IR coordinates by 1.9 arcsec, which is consistent with zero offset within

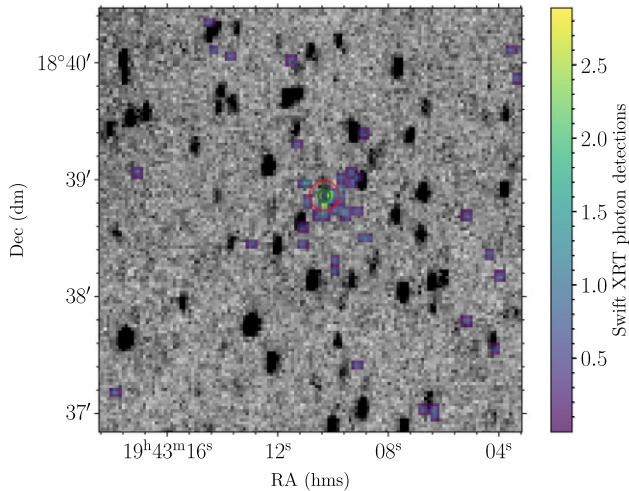


Figure 7. XRT photon-count mode image (blue/green/yellow) overlaid on a stacked UVOT *U*-band image (greyscale), Source 363 is located within the red (7.6 arcsec) and green (3.0 arcsec) annuli. These represent the source detection confidence radii (without and with UVOT astrometry, respectively), as calculated by ‘the *Swift*-XRT data products generator (Evans et al. 2014). Our system is faint in the stacked UV image, but the XRT image provides the first indication that the star is an X-ray source.

the uncertainties. We note that the rather scattered distribution of X-ray photons shown in Fig. 7 is typical of *Swift*/XRT observations of a single faint source; see https://www.swift.ac.uk/analysis/xrt/xrt_centroid.php for an example of how real sources are distinguished from noise.

Given the lower resolution of *Swift*’s instruments than the optical ones discussed thus far, the possibility of chance association should be considered. The measured X-ray flux is brighter than the *ROSAT* sensitivity limit (see below). Therefore we consider X-ray source density of 0.27 objects per deg² in the Galactic Plane, as determined from the *ROSAT* catalogue (Voges et al. 1999) at Galactic coordinates $30^\circ < l < 90^\circ$, $-3^\circ < b < 3^\circ$. With this figure the probability of a chance alignment within 3.0 arcsec is 3.78×10^{-6} . Given that the fitted XRT spectrum is brightest at the lower energy regime, the low sensitivity of *ROSAT* to higher energies is not detrimental to this estimation. Further to this, whilst there are two optical/IR sources within the XRT astrometric uncertainty radius, the associated UVOT light curve displayed high amplitude variability consistent with that observed in Source 363 and the second star is not optically variable. Therefore it is clear that the XRT X-ray source is Source 363.

The average count rate over the length of observations was $0.01375 \text{ counts s}^{-1}$; this was then converted into a flux via fitting an absorption adjusted power law to the XRT spectrum (see Section 2.4), with a model temperature of 20 keV. The previous lack of detections implied that the overall flux would be low, but our measured fluxes (adjusted for absorption) of $1.3_{-0.3}^{+0.4} \times 10^{-12} \text{ erg s}^{-1} \text{ cm}^{-2}$ are above the lower limits for surveys such as *ROSAT*, making the non-detection interesting. Luminosities corresponding to these fluxes have a range that is higher than average for IPs. Depending on the distance used, luminosity ranges from $6.9 \pm 1.8 \times 10^{31} \text{ erg s}^{-1}$ to $2.3 \pm 0.6 \times 10^{32} \text{ erg s}^{-1}$, at the closest and furthest distance estimates, respectively (as discussed in Section 2.1). The associated X-ray light curve shows only an intermittent signal, implying that the source has a more extreme bright to faint state ratio than other similar stars.

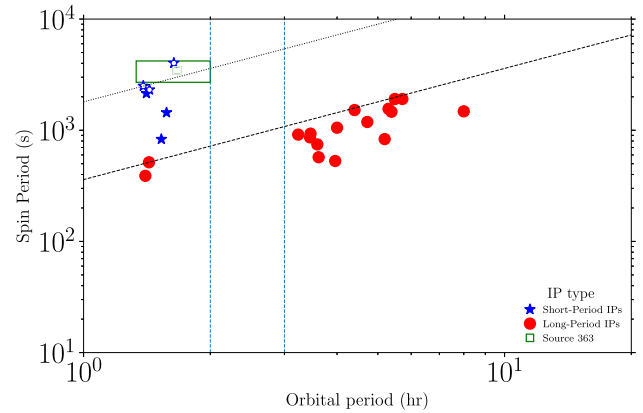


Figure 8. Orbital period versus spin period for a selection of known IPs (data from Mukai’s IPs – see Footnote no. 2). The blue stars represent short-period systems (those with white dots being mentioned in the text), red circles typical IPs. The green rectangle represents the likely range of orbital and spin periods of Source 363, these being constrained by the minimum orbital period of $\approx 80 \text{ min}$ (Knigge et al. 2011) and the lower limit of the period gap’. The two dashed vertical lines at $P_{\text{orb}} = 2$ and 3 h represent the ‘period gap’ where magnetic braking due to angular momentum transfer will cut-off mass transfer between the WD and its companion. The diagonal dashed line is where $P_{\text{orb}} = 10 \times P_{\text{spin}}$, below which long-period IPs are found. The additional dotted line demarcates the region where the orbital period is twice the spin period, which is a common feature of short-period IPs.

4 DISCUSSION

4.1 Comparison to sources in the literature

Existing IPs with some degree of similarity to Source 363 have often been detected either through their X-ray emission or optical narrow-band flux. Thus we must compare the overall behaviour of Source 363 to these systems (see Fig. 8), in order to understand the observed behaviour. Constructing some approximate optical to near-IR spectral energy distributions (SEDs; see Fig. 9), we note that Source 363 has both the lowest overall luminosity at the wavelengths measured and an unexpectedly faint optical SED. This SED has been formed by averaging all available measurements at each wavelength (including each individual measurement from this work, as well as all available archive data), with the full range of values also marked on the plot. It should be noted that the *J* ($1.25 \mu\text{m}$) and *H* ($1.65 \mu\text{m}$) data are single measurements that may not be representative: the *J* datum may be near a peak value, given the exceptionally blue *J* – *H* colour (see Section 1). Having noted this caveat, the SED appears to have a redder slope than other systems, possibly a by-product of the disc being optically thicker than other examples. The two most similar objects (EX Hya and DW Cnc) are both short-period systems that lack discs, and exist in a separate portion of the IP spin–orbit period diagram, where $P_{\text{orb}} \approx 2 \times P_{\text{spin}}$ (see Fig. 8),² as opposed to the more common ratio $P_{\text{orb}} \approx 10 \times P_{\text{spin}}$.

²References for Fig. 8: Hilton et al. (2009), Rodríguez-Gil et al. (2004), Andronov & Breus (2013), Buckley et al. (1998), Buckley & Tuohy (1989), Hellier (1993, 1997), Kemp et al. (2002), Norton et al. (2002), Staude et al. (2003), Woudt & Warner (2003), Woudt et al. (2012), Kim et al. (2005), Joshi, Ashok & Banerjee (2011), Masetti, Nucita & Parisi (2012), Mateo, Szkody & Garnavich (1991), Kaluzny & Semeniuk (1988), Burwitz et al. (1996), Evans, Hellier & Ramsay (2006), Pretorius (2009), Sazonov et al.

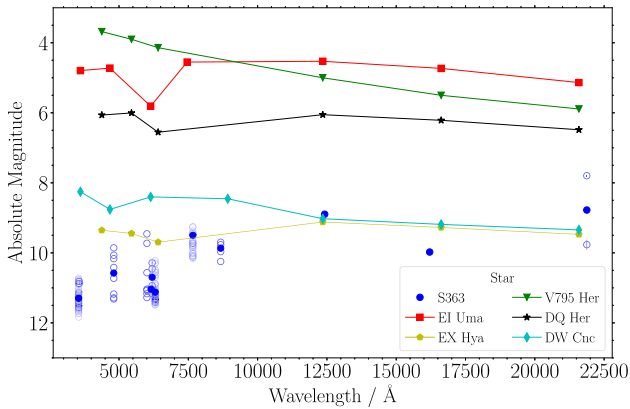


Figure 9. Optical and near-IR SEDs (AB system) for Source 363 (blue) and a selection of existing IPs from the literature. The solid blue points represent the median optical values from the new light curves in this work (u' , r' , i'), the three Pan-STARRS passbands, and two INT Galactic Plane Survey (IGAPS) passbands with multiple epochs: (g , r , z) and (u , r), respectively. The single-epoch J and H UKIDSS data and the mean of the two UKIDSS K values are also shown as solid blue points. Open circles are the individual measurements from which the medians were computed. (For readability the Pan-STARRS r , WHT r' , and IGAPS r data in slightly different filters have been offset by 250 Å, but u and u' are almost identical so they are combined into one average.) Note the high red optical and IR luminosity compared to shorter wavelengths. This is not present in previously classified IPs. The selected IPs are those with long spin periods and orbital periods ($P_{\text{spin}} \sim 0.3P_{\text{orb}}$), with distances coming from Bailer-Jones et al. (2021), using *Gaia* EDR3.

We propose that our source might also be a part of this small population, given the lack of a detectable short spin period in any of our observations, and the orbital period lower limit given the low mass of the companion (see Section 4.2). Our u' light curve is also similar in shape to DW Cnc (Rodríguez-Gil et al. 2004), although it is a factor of 2 higher in amplitude, with both sources having periods of under 1 h. The corresponding r' light curve from the same night of observations shares little in common with any typical IP system in the literature.

A more comparable object is the short-period IP V598 Peg (SDSS J233325.92+152222.1; Szkody et al. 2005; Southworth et al. 2007), which has a spin period of 43 min, and a confirmed (via *XMM-Newton* direct observations by Hilton et al. 2009) orbital period of 86 min. The shape of the optical light curve when phase folded (fig. 4 in Hilton et al. 2009) is almost identical to the r' -band curve (see Fig. 5). In addition, the $H\alpha$ to $H\beta$ ratio of 1.87 is of a similar order to Source 363.

To compare our spectrum to the literature, we find Oliveira et al. (2017) to be a good source of similar candidates due to their survey also using SOAR’s Goodman Spectrograph. Source 363’s slightly blue continuum (by comparison to polar-like sources) and broad lines bear the closest resemblance to MLS 2054–19, MLS 0720+17, CSS 1012–18, and SSS 1359–39 (see fig. 1 in the aforementioned paper). Interestingly, three of these are classified by those authors as discless IPs (MLS 0720+17 was suggested to be a polar). Some small differences to these sources are worth noting, in particular the relative strength of the $H\beta$ line compared to $H\alpha$, with all of these sources having the 4–2

(2008). The URL of the Mukai’s IPs (where this data is collated) is as follows: <https://asd.gsfc.nasa.gov/Koji.Mukai/iphome/iphome.html>

transition as strong or stronger than the 3–2 line, the inverse of our finding.

4.2 Nature of the system?

As it stands, we can say with some confidence that if the apparent ~ 45 –70 min variation time-scales are related to the WD spin period (e.g. with the spread of values caused by stochastic flickering), then the system cannot be a polar CV. All hydrogen-rich stars will overflow, rather than fill, their Roche lobes for such short periods (leading to a rapid cut-off of the mass transfer via magnetic braking), and the optical spectrum of the source clearly shows strong hydrogen emission lines, indicating that accretion is taking place. The argument could be made that there are two accretion streams, from both poles of the WD being magnetized (synchronizing the system) much like the system V2400 Oph (Hellier & Beardmore 2002), and thus the spin period would then be on the order of 90 min. However given that the spectrum suggests a disc, it is more likely the orbital period is longer than the spin period and just below ‘period gap’, making the system some form of IP.

With the IP explanation preferred based on the optical spectrum, it then becomes important to investigate the evolutionary state of the system, in order to explain the unusual behaviour (high amplitude, red SED, and low overall luminosity). We can add constraints to the orbital period of the system by considering its near-IR brightness and the amplitude of the associated variability; using the Bailer-Jones et al. (2021) *Gaia* EDR3 distance of $900.7_{-245.6}^{+288.3}$ pc, we find Source 363 has $M_K \approx 6$, and in order to explain the observed variability the companion object must be at least 1 mag fainter than that. This is because the variability is intrinsic to the WD, and thus the companion must not be providing the majority of the flux. These two factors combined lead us to place constraints on the classification of the companion, finding that it should be no more massive than an M3V star at 0.36 M_{\odot} (Pecaut & Mamajek 2013). This proposed limit on the companion mass would put the orbital period at roughly 2.5 h or less, where a 2.5 h period sits in the IP ‘period gap’. Equally using fig. 13 in Knigge et al. (2011) for our two K_s observations leads to orbital period limits of between 2.1 and 1.4 h. While this is a wide spread of values it does place the system below the period gap, in the region between that and the minimum IP orbital period of 80 min.

Thus we can reasonably then assume the orbital period is less than the 2.1 h lower limit (Rappaport, Joss & Webbink 1982), especially given the higher than average X-ray luminosity (stars within the gap have very low accretion rates, and thus low X-ray luminosity). Additionally a companion star of the described nature would have a short orbital period if in an IP-like system, lending further credence for Source 363 to exist below the period gap. There is an argument to be made that the orbital period is in fact less than 90 min, as can be seen in Fig. 8, because a number of short-period IPs (including the aforementioned V598 Peg) have settled into orbital periods at twice that of the WD spin, but with the same magnetic moment as more normal IPs, as predicted in Webbink & Wickramasinghe (2002). With an orbital period in this range we would expect a typical IP system to have a spin period on the order of 5–9 min, which is not seen in our data, hence we posit that Source 363 may be a member of the short-period subclass mentioned above. This would roughly place the spin period of the WD between 41 and 63 min, which mimics the time-scales observed in our optical data.

Finally, the observed strong IR excess (as described in Section 4.1) can then be assumed to be tracing the accretion flow, made more

likely due to the lack of cyclotron emission features in the optical spectrum. Combining this with the short period, we can infer that our system has a reasonably high accretion rate for its short-period type. The method for this accretion is still uncertain, but is could be novel; our light curves suggest direct accretion, whilst our SED and spectra suggest the presence of a disc, and thus disc-fed accretion. In order to make sense of this dichotomy, there is a possible explanation that Source 363 is currently undergoing an evolutionary transition between a typical (long-period) IP and the short-period systems, such as has been described by Southworth et al. (2007) and Norton et al. (2008).

There is currently an open question as to what the number density of short-period IPs should be (Pretorius & Mukai 2014). The small binary separations in short-period systems should easily allow the WD magnetic fields to connect with the convective donor star, and thus quickly synchronize the orbits, with system thus becoming a polar CV – provided $\mu_{\text{WD}} \lesssim 5 \times 10^{33} \text{ G cm}^3$ (Norton, Wynn & Somerscales 2004). This interpretation would render the subgroup short-lived, thus explaining their low observed numbers. On the other hand, WD magnetic fields can fall over time (Ohmic decay), and hence dramatically extend the time taken to become synchronous, in turn making such systems quite old, increasing the number density of this subgroup by extension. With a higher accretion rate than usual for short-period IPs, ram pressure would likely exceed magnetic pressure, which would then produce a disc, lending credence to this explanation for Source 363.

5 CONCLUSIONS

We report on the discovery of a new magnetic CV star system with an observed near-IR excess, and have determined that our source is most likely a short-period IP system, with a higher than average accretion rate. This decision was based upon the following.

(i) Our optical spectrum shows emission of H I, He I, and He II, all of which are indicators of magnetic CV systems. In addition the presence of disc-like features indicates that the magnetic field is not solely responsible for the accretion, making the case that the star is a polar unlikely.

(ii) The low optical luminosity of the system implies a low-mass companion to the WD, which sets an upper limit on the orbital period of the binary.

(iii) Combining this with the lack of an obvious spin period near the expected range of 5–9 min, we can infer that the system does not fit with the standard 1:10 ratio between spin and orbital time-scales. This deduction then places Source 363 within the loose group of short-period IPs, such as EX Hya.

(iv) The confirmed detection of X-ray emission from the system in targeted observations is interesting given that the star is absent from previous wide field X-ray surveys that cover the region (it does not feature in Pretorius et al. 2013). The non-detection by *ROSAT* would normally suggest that the overall X-ray luminosity is lower than typical IPs, a phenomenon that has been observed in other short-period systems. However, the measured X-ray luminosity of $1.31 \pm 0.34 \times 10^{32} \text{ erg s}^{-1}$ (using the *Gaia* EDR3 Bailer-Jones et al. 2021 estimated distance of 900 pc) is higher than that of most short-period IPs and we would expect the source to have been detected by *ROSAT*, if the luminosity were constant. We can then infer that this system goes through bright phases, relative to an otherwise faint X-ray flux level.

(v) Additionally, we make a case that given the short orbital period and low optical brightness, that the system has a lower than average

accretion rate (for an IP in general) and a companion star of a very faint type. This provides contrast with other short-period systems, making Source 363 seems fairly unique.

With such an unusual nature, implications from this work are twofold.

(i) It reiterates that there is a population of underluminous CVs that continue be missed in all wide area X-ray surveys completed thus far. But this work indicates a chance that the X-ray luminosity of these sources may not be as low as current literature suggests. Previous short-period systems have $L_X \approx 10^{31} \text{ erg s}^{-1}$, whereas Source 363 ($L_X \approx 10^{32} \text{ erg s}^{-1}$) shows that these systems can exist above this cut but still below the more usual value of $\approx 10^{33} \text{ erg s}^{-1}$ seen in typical IP systems. With the suggestions of a population of underluminous IPs that may be responsible for some of the observed X-ray excess in the galactic bulge (Hailey et al. 2016), Source 363 might be a useful laboratory to probe this idea further. The ongoing *eROSITA* (Predehl et al. 2021) survey should be deep enough to detect similar objects.

(ii) It shows the usefulness of using near-IR variability to locate this kind of object, as well as the benefits of multiwavelength astronomy to classify variable stars that are unexpected or unusual upon initial discovery.

The next steps in our investigation are to further constrain the system’s parameters, specifically the WD and companion masses, as well as the spin and orbital periods. In addition, having these parameters will allow us to test our ideas for the system’s unusual behaviour, as described in Section 4.2. In addition, we aim to find additional candidates within the VISTA Variables in the Via Lactea (VVV) survey (Minniti et al. 2010), via collation of short-period variable stars (Smith et al. 2018) with close distances and observed H α excess from the VST Photometric H α Survey of the Southern Galactic Plane and Bulge (VPHAS+; Drew et al. 2014). This will allow us to build an idea of the scale of this population, and thus the expected X-ray flux that would be produced. In turn, this would provide a useful metric to determine whether they are the cause of the aforementioned flux excess. Further the results thereof would indicate whether we are looking at a new subgroup of IPs or a short-lived phase in their evolution.

ACKNOWLEDGEMENTS

We acknowledge the use of public data from the *Swift* data archive. We also acknowledge the use of the WHT: the William Herschel Telescope and its service programme are operated on the island of La Palma by the Isaac Newton Group of Telescopes in the Spanish Observatorio del Roque de los Muchachos of the Instituto de Astrofísica de Canarias. We would like to thank the operations teams at both facilities for the quick and efficient observations.

CM acknowledges support from the UK’s Science and Technology Facilities Council (ST/S505419/1). NM and WJC are funded by University of Hertfordshire studentships; furthermore CM, PWL, NM, WJC, ZG, and JED recognize the computing infrastructure provided via STFC grant ST/R000905/1 at the University of Hertfordshire.

JS acknowledges support from the Packard Foundation and National Science Foundation grant AST-1714825. Portions of this work were performed while SJS held a NRC Research Associateship award at the Naval Research Laboratory. Work at the Naval Research Laboratory is supported by NASA DPR S-15633-Y.

ZG acknowledges the financial support from ANID (CONICYT) through the FONDECYT project No. 3220029.

DATA AVAILABILITY

All data are available from the first author upon request (and from PWL at p.w.lucas@herts.ac.uk), it will also be hosted at (star.herts.ac.uk/~cmorris/source_363_public/). *Swift* ToO data are publicly available at HEASARC.

REFERENCES

- Andronov I. L., Breus V. V., 2013, *Astrophysics*, 56, 518
 Astropy Collaboration et al., 2013, *A&A*, 558, A33
 Astropy Collaboration et al., 2018, *AJ*, 156, 123
 Atwood W. B. et al., 2009, *ApJ*, 697, 1071
 Bailer-Jones C. A. L., Rybizki J., Fouesneau M., Demleitner M., Andrae R., 2021, *AJ*, 161, 147
 Bonnardeau M., 2015, *Inf. Bull. Var. Stars*, 6146, 1
 Bradley L. et al., 2021, *astropy/photutils: 1.2.0 (1.2.0)*. Zenodo
 Bruch A., 2021, *MNRAS*, 503, 953
 Buckley D. A. H., Tuohy I. R., 1989, *ApJ*, 344, 376
 Buckley D. A. H., Cropper M., Ramsay G., Wickramasinghe D. T., 1998, *MNRAS*, 299, 83
 Burwitz V., Reinsch K., Beuermann K., Thomas H. C., 1996, *A&A*, 310, L25
 Chambers K. C. et al., 2016, preprint ([arXiv:1612.05560](https://arxiv.org/abs/1612.05560))
 Clemens J. C., Crain J. A., Anderson R., 2004, in Moorwood A. F. M., Masanori I., eds, *Proc. SPIE Vol. 5492, Ground-based Instrumentation for Astronomy*. SPIE, Bellingham, p. 331
 Contreras Peña C. et al., 2014, *MNRAS*, 439, 1829
 Drew J. E. et al., 2005, *MNRAS*, 362, 753
 Drew J. E. et al., 2014, *MNRAS*, 440, 2036
 Evans P. A., Hellier C., Ramsay G., 2006, *MNRAS*, 369, 1229
 Evans P. A. et al., 2009, *MNRAS*, 397, 1177
 Evans P. A. et al., 2014, *ApJS*, 210, 8
 Evans P. A. et al., 2020, *ApJS*, 247, 54
 Flewelling H., 2017, *Am. Astron. Soc. Meeting Abstr.*, #229, 237.07
 Gaia Collaboration et al., 2016, *A&A*, 595, A1
 Gaia Collaboration et al., 2018, *A&A*, 616, A1
 Gaia Collaboration et al., 2021, *A&A*, 649, A1
 Groot P. J. et al., 2009, *MNRAS*, 399, 323
 Hailey C. J. et al., 2016, *ApJ*, 826, 160
 Hellier C., 1993, *MNRAS*, 264, 132
 Hellier C., 1997, *MNRAS*, 288, 817
 Hellier C., Beardmore A. P., 2002, *MNRAS*, 331, 407
 Hilton E. J., Szkody P., Mukadam A., Henden A., Dillon W., Schmidt G. D., 2009, *AJ*, 137, 3606
 Joshi V. H., Ashok N. M., Banerjee D. P. K., 2011, *Bull. Astron. Soc. India*, 39, 259
 Kaluzny J., Semeniuk I., 1988, *Inf. Bull. Var. Stars*, 3145, 1
 Kemp J., Patterson J., Thorstensen J. R., Fried R. E., Skillman D. R., Billings G., 2002, *PASP*, 114, 623
 Kim Y. G., Andronov I. L., Park S. S., Jeon Y. B., 2005, *A&A*, 441, 663
 Knigge C., Baraffe I., Patterson J., 2011, *ApJS*, 194, 28
 Lacy M. et al., 2020, *PASP*, 132, 035001
 Littlefield C., Garnavich P., Kennedy M. R., Patterson J., Kemp J., Stiller R. A., Boardman J., Pellett E., 2020, *ApJ*, 896, 116
 Littlefield C., Scaringi S., Garnavich P., Szkody P., Kennedy M. R., Hkiewicz K., Mason P. A., 2021, *AJ*, 162, 49
 Lucas P. W. et al., 2008, *MNRAS*, 391, 136
 Lucas P. W. et al., 2017, *MNRAS*, 472, 2990
 Masetti N., Nucita A. A., Parisi P., 2012, *A&A*, 544, A114
 Mateo M., Szkody P., Garnavich P., 1991, *ApJ*, 370, 370
 Minniti D. et al., 2010, *New Astron.*, 15, 433
 Monguió M. et al., 2020, *A&A*, 638, A18
 Norton A. J., Quaintrell H., Katajainen S., Lehto H. J., Mukai K., Negueruela I., 2002, *A&A*, 384, 195
 Norton A. J., Wynn G. A., Somerscales R. V., 2004, *ApJ*, 614, 349
 Norton A. J., Butters O. W., Parker T. L., Wynn G. A., 2008, *ApJ*, 672, 524
 Oliveira A. S., Rodrigues C. V., Cieslinski D., Jablonski F. J., Silva K. M. G., Almeida L. A., Rodríguez-Ardila A., Palhares M. S., 2017, *AJ*, 153, 144
 Pecaut M. J., Mamajek E. E., 2013, *ApJS*, 208, 9
 Predehl P. et al., 2021, *A&A*, 647, A1
 Pretorius M. L., 2009, *MNRAS*, 395, 386
 Pretorius M. L., Mukai K., 2014, *MNRAS*, 442, 2580
 Pretorius M. L., Knigge C., Schwobe A. D., Pretorius M. L., Knigge C., Schwobe A. D., 2013, *MNRAS*, 432, 570
 Rappaport S., Joss P. C., Webbink R. F., 1982, *ApJ*, 254, 616
 Rodríguez-Gil P., Gänsicke B. T., Araujo-Betancor S., Casares J., 2004, *MNRAS*, 349, 367
 Sazonov S., Revnivtsev M., Burenin R., Churazov E., Sunyaev R., Forman W. R., Murray S. S., 2008, *A&A*, 487, 509
 Schreiber M. R., Belloni D., Gänsicke B. T., Parsons S. G., Zorotovic M., 2021, *Nat. Astron.*, 5, 648
 Silber A. D., 1992, PhD thesis, Massachusetts Institute of Technology (MIT), Cambridge, MA
 Skrutskie M. F. et al., 2006, *AJ*, 131, 1163
 Smith L. C. et al., 2018, *MNRAS*, 474, 1826
 Southworth J., Gänsicke B. T., Marsh T. R., de Martino D., Aungwerrojwit A., 2007, *MNRAS*, 378, 635
 Staude A., Schwobe A. D., Krumpke M., Hambaryan V., Schwarz R., 2003, *A&A*, 406, 253
 Szkody P. et al., 2005, *AJ*, 129, 2386
 Tody D., 1986, in Crawford D. L., ed., *Proc. SPIE Vol. 627, Instrumentation in Astronomy VI*. SPIE, Bellingham, p. 733
 Virtanen P. et al., 2020, *Nat. Methods*, 17, 261
 Voges W. et al., 1999, *A&A*, 349, 389
 Warner B., 1995, *Cataclysmic Variable Stars*. Cambridge Univ. Press, Cambridge
 Webbink R. F., Wickramasinghe D. T., 2002, *MNRAS*, 335, 1
 Woudt P. A., Warner B., 2003, *MNRAS*, 339, 731
 Woudt P. A. et al., 2012, *MNRAS*, 427, 1004

This paper has been typeset from a $\text{\TeX}/\text{\LaTeX}$ file prepared by the author.